PAIN® 154 (2013) 434–448

www.elsevier.com/locate/pain

Suppression of KCNQ/M (Kv7) potassium channels in dorsal root ganglion neurons contributes to the development of bone cancer pain in a rat model

Qin Zheng [a], Dong Fang [a], Min Liu [a], Jie Cai [a], You Wan [b], Ji-Sheng Han [a,b], Guo-Gang Xing [a,b,*]

[a] Neuroscience Research Institute and Department of Neurobiology, Peking University, Beijing, PR China
[b] Key Laboratory for Neuroscience of the Ministry of Education and the Ministry of Public Health, Beijing, PR China

Sponsorships or competing interests that may be relevant to content are disclosed at the end of this article.

ARTICLE INFO

Article history:
Received 1 May 2012
Received in revised form 5 November 2012
Accepted 6 December 2012

Keywords:
Bone cancer pain
Dorsal root ganglion
Hyperexcitability
KCNQ channel
M current
Retigabine
XE-991

ABSTRACT

Bone cancer pain has a strong impact on the quality of life of patients, but is difficult to treat. Better understanding of the pathogenic mechanisms underlying bone cancer pain will likely lead to the development of more effective treatments. In the present study, we investigated whether inhibition of KCNQ/M channels contributed to the hyperexcitability of primary sensory neurons and to the pathogenesis of bone cancer pain. By using a rat model of bone cancer pain based on intratibial injection of MRMT-1 tumour cells, we documented a prominent decrease in expression of KCNQ2 and KCNQ3 proteins and a reduction of M-current density in small-sized dorsal root ganglia (DRG) neurons, which were associated with enhanced excitability of these DRG neurons and the hyperalgesic behaviours in bone cancer rats. Coincidently, we found that inhibition of KCNQ/M channels with XE-991 caused a robust increase in the excitability of small-sized DRG neurons and produced an obvious mechanical allodynia in normal rats. On the contrary, activation of the KCNQ/M channels with retigabine not only inhibited the hyperexcitability of these small DRG neurons, but also alleviated mechanical allodynia and thermal hyperalgesia in bone cancer rats, and all of these effects of retigabine could be blocked by KCNQ/M-channel antagonist XE-991. These results suggest that repression of KCNQ/M channels leads to the hyperexcitability of primary sensory neurons, which in turn causes bone cancer pain. Thus, suppression of KCNQ/M channels in primary DRG neurons plays a crucial role in the development of bone cancer pain.

1. Introduction

Bone cancer pain resulting from primary tumours or tumours that metastasize to bone is one of the most severe and intractable types of cancer pain, which reduces the quality of life of patients [33,36]. Bone cancer pain generally consists of ongoing pain and breakthrough or incident pain [48,51,70], which are characterized by pathological symptoms, such as spontaneous pain, hyperalgesia, and allodynia [44,67]. The mechanism underlying the development of bone cancer pain still remains largely unknown.

Recently, we and others have found that the thermal hyperalgesia and mechanical hypersensitivity in murine models of bone cancer pain are associated with increased excitability of primary afferent neurons that innervate the tumour-bearing limb [25,34,78,79]. On the other hand, it has been documented that KCNQ/M (Kv7) voltage-gated potassium (K^+) channels play an essential role in setting the resting membrane potential and in controlling the neuronal excitability [9,74]. The KCNQ/M (Kv7) channels are a family of five voltage-gated K^+ channel subunits (Kv7.1 to Kv7.5) encoded by the *KCNQ1–5* genes [74]; among those, KCNQ2 and KCNQ3 are expressed exclusively in the nervous system [6,35], and coassembled KCNQ2 and KCNQ3 subunits are thought to constitute the native M channel in most neurons [71]. This channel generates a species of low-threshold, slowly activating, slowly deactivating, and noninactivating K^+ current (the M current), which acts as a brake to regulate the action potential (AP) firing and the neuronal excitability [9]. Consequently, suppression of M currents increases the neuronal excitability [9,45,64], whereas their enhancement has a silencing effect [20,24,26,27].

To date, a growing body of evidence also shows that nociception can be modulated by KCNQ/M channels [7,20,50,53], which are expressed at a number of key locations in the pain transmission pathway, including the nociceptive dorsal root ganglia (DRG) neurons [9,14,53,62]. For example, functional studies have shown that firing in these neurons can be inhibited by KCNQ/M-channel activators [20,39,53,57,58,61]. Therefore, retigabine, a specific KCNQ/M-channel opener, exerts an analgesic action in several models of neuropathic pain [7,17,50,72], inflammatory pain [9,42,53],

* Corresponding author at: Neuroscience Research Institute, Peking University, 38 Xue-Yuan Road, Beijing 100191, PR China. Tel./fax: +86 10 8280 1067.
E-mail address: ggxing@bjmu.edu.cn (G.-G. Xing).

0304-3959/$36.00
http://dx.doi.org/10.1016/j.pain.2012.12.005

and visceral pain [5,29,73], and these effects of retigabine can be reversed by KCNQ/M-channel blocker such as linopirdine or XE-991 [7,17,42,53,73]. These findings suggest that the KCNQ/M-potassium channel plays a key role in regulating the nociceptive transmission and may therefore contribute to the development of chronic pathologic pain, such as inflammatory or neuropathic pain. However, the potential roles of KCNQ/M channels in the development of bone cancer pain are largely unclear.

In this study, we investigated whether inhibition of KCNQ/M channels contributed to the hyperexcitability of primary sensory neurons and to the pathogenesis of bone cancer pain. Our results show that implantation of MRMT-1 tumour cells into the tibial canal in rats produces a prominent repression of KCNQ/M channels in small-sized DRG neurons, which is associated with the enhanced neuronal excitability and the hyperalgesic behaviours in bone cancer rats. These data imply that suppression of KCNQ/M channels leads to the hyperexcitability of primary sensory neurons, which in turn causes the development of bone cancer pain.

2. Materials and methods

2.1. Animals

Adult Sprague-Dawley rats weighing 180 to 220 g at the beginning of the experiment were provided by the Department of Experimental Animal Sciences, Peking University Health Science Center. The rats were housed in separated cages with free access to food and water. The room temperature was kept at 24°C ± 1°C under natural light–dark cycle. All animal experimental procedures were carried out in accordance with the guidelines of the International Association for the Study of Pain [80] and were approved by the Animal Care and Use Committee of Peking University. The behavioural experimenters were kept blind from the groupings of the rats.

2.2. Bone cancer pain model

A rat model of bone cancer pain was established by intratibial injections of syngeneic MRMT-1 rat mammary gland carcinoma cells as previously described [47]. Briefly, after being anesthetized with chloral hydrate (0.3 g/kg, intraperitoneally), the rat left tibia was carefully exposed and a 23-gauge needle was inserted into the intramedullary canal of the bone. It was then removed and replaced with a long, thin blunt needle attached to a 10-μL Hamilton syringe containing the medium to be injected. A volume of 4 μL MRMT-1 rat mammary gland tumour cells (4×10^4), inactivated (heat-killed) tumour cells, or vehicle (phosphorylated buffer solution [PBS]) was injected into the tibial bone cavity. After injection the site was sealed with bone wax, and the wound was finally closed.

To assess the bone destruction after tumour cell inoculation, tibia bone radiographs and histological staining were performed in this study. On days 7, 14, 21, and 28 after tumour cell inoculation, tibial bone radiographs from hind limbs of MRMT-1-treated, inactivated MRMT-1-treated, and vehicle (PBS)-treated rats, as well as naive rats (n = 4 for each group), were taken using a Digital Radiographer System (DR7000, Eastman Kodak Company, Rochester, NY). Radiographic images of the tibia bones were assessed for extent of destruction as previously described [68]. After radiological examination, bilateral tibia bones were processed for paraffin embedding as described elsewhere [63]. Briefly, rats were anesthetized with an overdose of sodium pentobarbital and transcardially perfused with 300 mL of 0.9% normal saline followed by 300 mL 4% paraformaldehyde. Bilateral tibia bones were removed and fixed in a 1:500 zinc-buffered formalin solution overnight at 4°C and then decalcified in 10% ethylene-diamine-tetra acetic acid solution for 14 days. The bones were rinsed, dehydrated, and then embedded in paraffin, cut into 7-μm cross-sections using a rotary microtome (Reichert-Jung 820, Cambridge Instruments, Nussloch, Germany), and stained with hematoxylin and eosin to visualize the extent of tumour infiltration and bone destruction.

2.3. Behavioural studies

2.3.1. Assessment of mechanical allodynia

Mechanical allodynia, as a behavioural sign of bone cancer pain, was assessed by measuring 50% paw withdrawal threshold (PWT) as described in our previous reports [23,55]. The 50% PWT in response to a series of von Frey filaments (Stoelting, Wood Dale, IL) was determined by the Up and Down method [11]. The rat was placed on a metal mesh floor covered with an inverted clear plastic cage (18 × 8 × 8 cm) and allowed a 20-minute period for habituation. Eight von Frey filaments with approximately equal logarithmic incremental (0.224) bending forces were chosen (0.41, 0.70, 1.20, 2.00, 3.63, 5.50, 8.50, and 15.10 *g*). Each trial started with a von Frey force of 2.00 *g* delivered perpendicularly to the plantar surface of the left hindpaw for about 2 to 3 seconds. An abrupt withdrawal of the foot during stimulation or immediately after the removal of the hair was recorded as a positive response. Whenever there was a positive or negative response, the next weaker or stronger filament was applied, respectively. This procedure was done until 6 stimuli after the first change in response had been observed. The 50% PWT was calculated using the following formula: 50% PWT = $10^{[X_f+k\delta]}$, where X_f is the value of the final von Frey filament used (in log units), k is a value measured from the pattern of positive/negative responses, and $\delta = 0.224$, which is the average interval (in log units) between the von Frey filaments [15]. If an animal responded to the lowest von Frey filament, a value of 0.25 *g* was assigned. If an animal did not respond to the highest von Frey filament, the value was recorded as 15.0 *g*. Testing sessions were performed on the day before injection and on days 1, 3, 7, 10, 14, 21, and 28 after cancer cells or sham injection. The mechanical allodynia was assessed by measuring 50% PWT of ipsilateral hind paw in tumour cells and in sham-operated rats, respectively.

2.3.2. Assessment of thermal hyperalgesia

Thermal hyperalgesia of the hind paws was tested as described by our previous report [55]. Rats were allowed to acclimate for a minimum of 30 minutes within acrylic enclosures on a clear glass plate maintained at 30°C. A radiant heat source was focused onto the plantar surface of the hind paw. Measurements of paw withdrawal latency (PWL) were taken by a timer that was started by the activation of the heat source and stopped when withdrawal of the paw was detected with a photo detector. A maximal cutoff time of 30 seconds was used to prevent unnecessary tissue damage. Three measurements of PWL were taken for each hind paw and were averaged as the result of each test session. The hind paw was tested alternately with >5 minute intervals between consecutive tests.

2.3.3. Measurement of drug effects on pain behaviours

The first behavioural experiment was performed to examine whether inhibition of KCNQ/M channels with XE-991 produced nociceptive behaviours in normal rats. Effects of XE-991 at various doses of 0.25, 0.5, 0.75, and 1.0 mg/kg were measured at 30, 60, 90, 120, and 150 minutes after intraperitoneal injection, respectively. The second experiment was carried out to determine whether activation of the KCNQ/M channels by using its specific opener retigabine attenuated the hyperalgesic behaviours in a rat model of bone cancer pain, and whether the effects of retigabine could be reversed by KCNQ/M-channel blocker XE-991. On day 14 after tumour cell inoculation, rats with bone cancer pain, confirmed by measuring the mechanical allodynia and thermal hyperalgesia,

were intraperitoneally administrated with retigabine, retigabine plus XE-991, or vehicle 30 minutes before assessing the effects of reagents on signs of bone cancer pain (mechanical allodynia and thermal hyperalgesia). Here, retigabine was used at a dose of 8 mg/kg and XE-991 at 1 mg/kg. The dose-dependent responses of retigabine on pain behaviours were assessed at doses of 2, 4, 6, and 8 mg/kg, and the retigabine effects were measured at 30, 60, 90, 120, and 150 minutes after injection at each dose, respectively. Retigabine or XE-991 used in this study was dissolved in the same vehicle, which was a mixture of 10%Tween-80 in normal saline solution.

2.4. Immunohistochemistry

Deeply anesthetized rats were intracardially perfused with 50 mL of 0.1 M phosphate buffer (PB) followed by 500 mL of 4% paraformaldehyde (in 0.1 M PB, pH 7.4). The left L4 and L5 DRG were quickly removed, postfixed in the same fixative solution for 2 hours and then were cryoprotected in 30% sucrose (in 0.1 M PB). Several days later, the tissues were sectioned in 8-μm thickness on a cryostat. After blocking in 10% normal goat serum for 1 hour, the sections were incubated with affinity-purified rabbit antibody to KCNQ2 or KCNQ3 (1:500, Abcam, Cambridge, MA) at 4°C overnight. Control sections were processed without the addition of primary antibody. The sections were then washed in 0.1 M PBS and incubated with biotinylated goat antirabbit immunoglobulin G (1:300, Invitrogen, Carlsbad, CA) at 37°C for 30 minutes. After several washes in PBS, the sections were incubated in the avidin-biotin-peroxidase complex (1:300, ABC Elite, Invitrogen) at 37°C for 45 minutes. The horseradish peroxidase reaction was developed in 0.1 M Tris-buffered saline (pH 7.4) containing 0.05% 3, 3P-diaminobenzidine and 0.01% H_2O_2. The sections were then dehydrated and coverslipped. Absorption control using an immunizing peptide blocking experiment and blank control omitting the primary antibody were performed in our experiments.

Absorption controls using an immunizing peptide blocking experiment were performed according to the manufacturer's instructions. Briefly, before proceeding with the staining protocol, the antibody was neutralized, ie, incubated with an excess of peptide that corresponds to the epitope recognized by the antibody. Here, the immunogen for anti-KCNQ2 (ab22897) antibody is from a.a. 858-872. For anti-KCNQ3 (ab66640) antibody, the immunogen sequence is located within a.a. 800 and 872 of the KCNQ3 human protein. Thus, synthetic KCNQ2 peptide (1:400, Abcam) derived from within residues 850 to the C-terminus of KCNQ2, and KCNQ3 peptide (1:300, Abcam) from within residues 800 to the C-terminus of KCNQ3. The antibody that was bound to the blocking peptide was no longer available to bind to the epitope present in the protein in the cell. The neutralized antibody was then used side by side with the antibody alone, and the results were compared. By comparing the staining from the blocked antibody vs the antibody alone, the specific staining could be determined: this staining was absent from the immunostaining performed with the neutralized antibody (Supplementary Fig. S1).

For relative quantification of immunoreactivity, a computer-assisted image analyzer (Image Pro Plus, version 6.0, Media Cybernetics, Silver Spring, MD) was used at a magnification of ×20. Image was acquired using a cooled CCD camera (Spot 2; Diagnostic Instruments, Sterling Heights, MI), mounted on a Leica DMI3000 B microscope (Leica, Wetzlar, Germany). The ratio of KCNQ2 (or KCNQ3)-positive cells compared with the total neuronal profiles and the average intensity of KCNQ2 (or KCNQ3)-positive neuronal profiles of DRG were calculated in a blind fashion to identify any relative changes in KCNQ2 (or KCNQ3) expression in the DRG neurons. The average intensity was defined as the difference between average gray value (mean integrated optical density) within each DRG section and its background. For calculating the percentage of KCNQ2 (or KCNQ3)-positive neuronal profiles, approximately 500 neuronal profiles from 5 consecutive sections (80-μm interval) of each L4 or L5 DRG of each animal were analyzed. Each threshold density in the DRG was determined for positive immunoreactivity above background, and the thresholds were kept constant for all samples. Neurons that had densities higher than a threshold density were considered to show positive expression. A mean value was calculated for each DRG, and all individual values for each DRG at each time point were averaged to provide a single mean ± SEM. Profiles of the DRG neurons were categorized by size: small (area <600 μm^2), medium (area 600 to 1200 μm^2), and large (area >1200 μm^2).

2.5. Western blot

Rats were deeply anesthetized with 10% chloral hydrate (0.3 g/kg, intraperitoneally) and then the L4 and L5 DRG were removed and immediately homogenized in ice-chilled lysis buffer containing 50 mM Tris (pH 7.5), 250 mM NaCl, 10 mM ethylenediaminetetraacetic acid (pH 8.0), 0.5% NP40 (Sigma, St. Louis, MO), 1 mM phenylmethanesulfonyl fluoride (Sigma), 4 mM Sodium Fluoride (NaF). The homogenates were centrifuged at 1200 *g* for 10 minutes at 4°C, and the supernatant was analyzed. The concentration of protein was measured with a BCA assay kit (Pierce, Rockford, IL), and equal amount of protein samples (20 μg) were denatured and then separated through sodium dodecyl sulphate-polyacrylamide gel electrophoresis using 10% running gels and transferred to a polyvinylidene difluoride filters membrane (Bio-Rad, Hercules, CA). After blocking with 5% nonfat milk in TBST (20 mM Tris-HCl, pH 7.5, 150 mM NaCl, and 0.05% Tween-20) for 60 minutes at room temperature, the membranes were incubated with primary antibody, rabbit anti-KCNQ2 or KCNQ3 (1:1000, Abcam), or mouse anti–glyceraldehyde 3-phosphate dehydrogenase (1:1000, Biodesign, Saco, Maine, USA), at 4°C overnight. The blots were washed in TBST and then incubated in horseradish peroxidase–conjugated secondary antibody (1:1000, goat antirabbit or mouse, Jackson, West Grove, Pennsylvania, USA). Protein bands were visualized using an enhanced chemiluminescence detection kit (ECL, Santa Cruz Biotechnology, Inc., Santa Cruz, CA, USA) followed by autoradiography using Hyperfilm MP (Santa Cruz). The standardized ratio of KCNQ2 (or KCNQ3) to glyceraldehyde 3-phosphate dehydrogenase band density was used to calculate the alteration in KCNQ2 (or KCNQ3) expression.

2.6. Whole-cell patch-clamp recordings

Neurons were isolated from L4 and L5 DRG of adult rats using methods as previously described [12]. Briefly, freshly dissected ganglia were minced and washed in cold, oxygenated Dulbecco Modified Eagle Medium (DMEM; Sigma), and were then subjected to collagenase (3 mg/mL, type IA, Sigma) treatment for 45 minutes, followed by trypsin (2 mg/mL, Type II-S, Sigma) for 15 minutes at 37°C. The enzymatic reaction was stopped by washing the cells with DMEM containing 10% fetal bovine serum, and the remaining pieces of ganglia were gently triturated by using a fire-polished glass Pasteur pipette and passed through a 40-μm cell strainer. The suspension was then centrifuged at 800 rpm for 3 minutes, and the cell pellet was resuspended in fresh DMEM supplemented with 10% fetal bovine serum. The dissociated cells were placed on poly-D-lysine (0.1 mg/mL, Sigma)-treated glass coverslips contained within 4-well sterile tissue culture plates and kept in 5% CO_2 incubator at 37°C for 2 to 3 hours before recording.

Whole-cell voltage- and current-clamp recordings were performed at room temperature using an EPC-10 amplifier and Patchmaster software (HEKA, Lambrecht/Pfalz, Germany). Patch pipettes were pulled from borosilicate glass capillaries with a tip resistance

of 5 to 8 MΩ when filled with internal solution containing (in mM) 80 K-acetate, 30 KCl, 40 2-[4-(2-hydroxyethyl)-1-piperazinyl] ethanesulfonic acid (HEPES), and 1 $CaCl_2$, adjusted to pH 7.4 with potassium hydroxide (KOH). The external solution contained (in mM) 144 NaCl, 2.5 KCl, 2 $CaCl_2$, 0.5 $MgCl_2$, 5 HEPES, and 10 glucose, adjusted to pH 7.4 with NaOH. Drugs were prepared in the external solution and delivered by a gravity-fed multibarrel perfusion system (VaveLink 8; Automate Scientific, Berkeley, CA). Membrane currents and APs were measured with pipette and membrane capacitance cancellation, filtered at 2 kHz, and digitized at 10 kHz. Series resistance was compensated 70% to 90%. The membrane capacitance was read from the amplifier by the software Patchmaster for determining the size of cells and calculating the current density. In this study, small-sized DRG neurons defined by their diameters (⩽30 μm) and C_m (⩽28.3 pF) as described in a previous report [30] were performed by electrophysiological studying.

For current-clamp recording, the cells were held at 0 pA, and the firing threshold of DRG neurons was first measured by a series of 100-ms depolarizing current injection in 5-pA steps from 0 pA to elicit the first AP. To further examine the neuron firing properties, a depolarizing current pulse (1-second, 2-fold AP threshold) was delivered to elicit the cell generating sufficient firing. In some experiments, a large depolarizing current of 1 second, 300 pA was also delivered to ensure that all recorded neurons could be evoked firing and the evoked discharges were elicited under an equal depolarizing current pulse. We have demonstrated that this depolarizing current pulse (1 second, 300 pA) could evoke APs firing in all recorded small DRG neurons in our preliminary experiments. A hyperpolarizing current injection in 200 ms, −200 pA was used to measure membrane input resistance (R_{in}), which was assessed from the value of the evoked membrane potential divided by the injected hyperpolarizing current (−200 pA). In some experiments, the following electrophysiological baseline properties of cells were measured in this study: resting membrane potential (RMP); the depolarized current threshold for eliciting the first AP; threshold potential (TP); rise rate of TP ([RMP-TP]/duration from RMP to TP); amplitude, overshot, and duration of AP; rise and fall time of AP as well as frequency of AP; interspike intervals (ISI); amplitude of afterhyperpolarization (AHP) and AHP duration at 80% repolarization ($AHP_{80\%}$).

For voltage-clamp recordings, M currents in DRG cells were studied by holding the membrane potential at −20 mV and applying a 1-second hyperpolarizing pulse from −20 mV to −110 mV in increments of −10 mV at 4 second-intervals. The M current was defined as the outward current sensitive to 3 μM XE-991, and the amplitude of M currents was measured from deactivation current records at −50 mV as the difference between the average of a 10-ms segment, taken 10 to 20 ms into the hyperpolarizing step, and the average during the last 10 ms of that step [65]. Mean instantaneous and steady-state I–V relationships for M current were obtained by measuring the current at the beginning and end of the voltage pulse, respectively. Deactivation of M current was best-fitted by 2 exponentials, with 2 time constants, τ_{fast} and τ_{slow}. Concentration response curves for XE-991 were constructed by plotting percentage inhibition of M current as a function of drug concentration plotted on a log scale. Smooth curves were fitted to these data with the Hill equation of the form $y = y_{max}\, x^n/(k^n + x^n)$, where x is the concentration, y is the percentage inhibition, and y_{max} is the maximal value of y (at saturation); in the fitting procedure y_{max} was constrained not to exceed 100%. The term k is the IC_{50} (the concentration giving half-maximal inhibition) and n (Hill slope) is the power term related to the slope of the curve. The program Origin (version 8.0; Microcal Software, Northampton, MA) was used for creating the figures.

2.7. Reagents

Retigabine (N-(2-amino-4-(4-fluorobenzylamino)-phenyl) carbamic acid ethyl ester) was purchased from Melone Phamaceutical Co., Ltd (Danlian, China). XE-991 (10, 10-bis (4-pyridinylmethyl)-9(10H)-anthracenone) was purchased from Tocris (Ellisville, MO). Both were dissolved in 10% Tween-80 as a 10-mM stock solution, stored at −20°C, and diluted to desired concentrations just before experiments. All other chemicals or reagents were obtained from Sigma, Invitrogen, or Abcam except as mentioned in the text.

2.8. Statistical analysis

Statistical analyses were performed with GraphPad Prism 5 for Windows (GraphPad Software, La Jolla, CA). All data were expressed as mean ± SEM. The two-tailed Student t test was used for the comparison of the mean values between two groups. One-way analysis of variance (ANOVA) followed by the Dunnett multiple comparison test or two-way ANOVA followed by Bonferroni post hoc test was used for multiple comparison. Differences with $P < .05$ were considered statistically significant.

3. Results

3.1. Radiological and histological evaluation of tumour growth and bone destruction

The tumour growth and bone destruction were evaluated using radiological and histological methods. Radiographs showed extensive damage to the cortical bone and the trabeculae by day 7 to 14 after inoculation of tumour cells, and by day 21, the damage was threatening the integrity of the tibial bone. By day 28, further deterioration was detected with medullary bone loss and full thickness bicortical bone loss. No radiological change was observed on contralateral tibia bone up to 28 days after inoculation. Similarly, no radiological change was found in naïve animals, in animals treated with heat-killed tumour cells, or with PBS. Representative examples are presented in Fig. 1.

Sections obtained from the proximal end of the tibia on day 7, 14, 21, and 28 after inoculation were stained with hematoxylin and eosin. Histological staining showed that on day 28 after inoculation, tumour growth and various degrees of bone destruction were observed in animals that received live MRMT-1 tumour cells. Remodelling of the bone was also observed in the affected bone. In cases of severe bone destruction, the tumour destroyed bone matrix and periosteum and grew outside of the bone. In contrast, no tumour growth or bone destruction was observed in naïve animals or in the animals that received heat-killed tumour cells or PBS (Fig. 2).

3.2. Tumour-evoked mechanical allodynia and thermal hyperalgesia

As in our recent report [79], implantation of MRMT-1 tumour cells into the tibial canal in rats produced significant mechanical allodynia and thermal hyperalgesia (Supplementary Fig. S2). Both PWT to von Frey filament and PWL to radiant heat decreased significantly from day 10 to day 28 after inoculation of tumour cells in ipsilateral hind paw of MRMT-1 rats, whereas no significant alteration was observed in heat-killed (HK) tumour cells or PBS inoculation rats. Altogether, the aforementioned data suggested the development of bone cancer–induced pain in MRMT-1 rats (for reference, see our recent publication [79]).

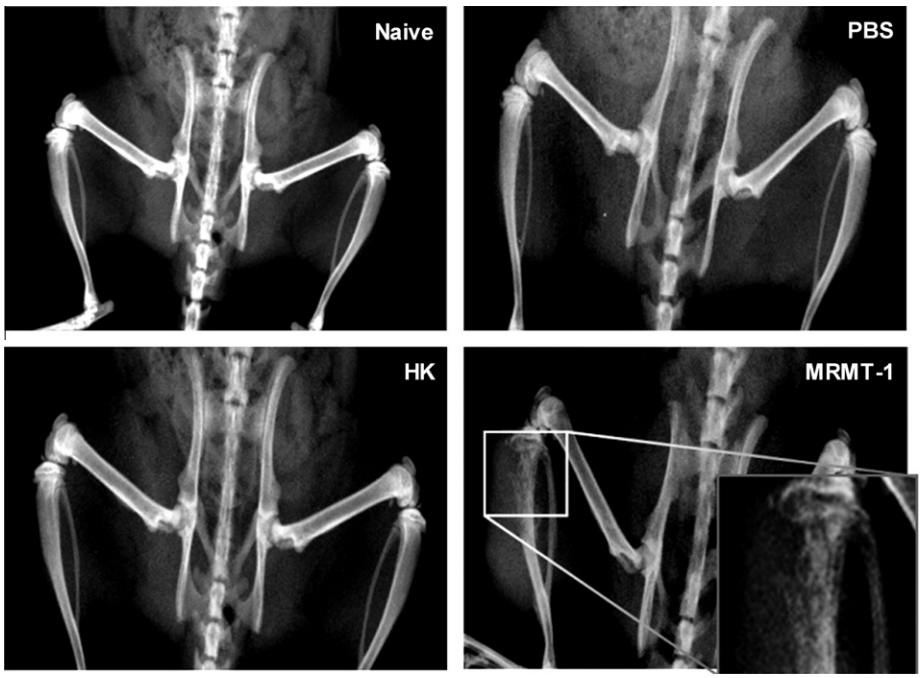

Fig. 1. Radiographs of the rat tibial bone implanted with phosphorylated buffer solution (PBS), heat-killed (HK) MRMT-1 cells, or live MRMT-1 cells (4×10^4) on day 28 after inoculation. The PBS, HK, or live MRMT-1 cells were injected into the left tibial bone cavity. The higher magnification of the proximal third of the bones from MRMT-1 rats (in the square box) is shown in the bottom right. Note that severe deterioration with medullary bone loss and full-thickness bicortical bone loss was observed on ipsilateral but not contralateral tibia bone in rats with live MRMT-1 cell inoculation. No radiological change was found in naïve rats or in rats with HK tumour cells or PBS injection.

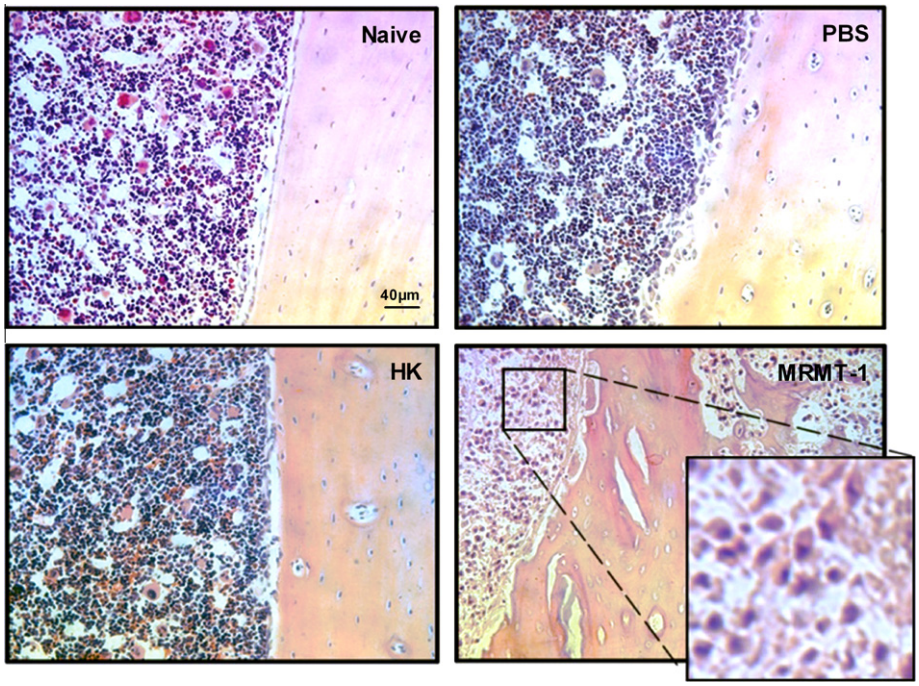

Fig. 2. Histology (hematoxylin-eosin staining) of the rat tibial bone implanted with phosphorylated buffer solution (PBS), heat-killed (HK) MRMT-1 cells, or live MRMT-1 cells on day 28 after inoculation. Note that the tumour growth and bone destruction appeared after being injected with live MRMT-1 cells, but not with PBS or HK MRMT-1 cells. The higher magnification from MRMT-1 rats (in the square box) is shown in the bottom right. The histology of the tibial bone from naïve rats is shown in the top left. Scale bar = 40 μm.

3.3. Increase in excitability of small-sized DRG neurons in bone cancer rats

Furthermore, we examined spontaneous activities and evoked discharges in small-sized DRG neurons (capacitance 18.2 ± 0.2 pF; range 12.5–24.9 pF; n = 215) in naïve, PBS, HK, and MRMT-1-rats. As reported in our previous studies [79], implantation of tumour cells into the rat tibial canal provoked more spontaneous discharges and evoked tonic discharges (Supplementary Fig. S3), and increased frequency of evoked APs (Supplementary Fig. S4)

in small DRG neurons, accompanied by alterations in intrinsic membrane properties that reflect the enhanced neuronal excitability, including depolarized RMP, reduction in current threshold and voltage threshold (TP) of AP, and decrease in amplitude, overshot, and duration of evoked APs as well as in amplitude and duration of AHP (Supplementary Table S1). Moreover, we also observed that more DRG neurons exhibit subthreshold membrane potential oscillations in MRMT-1 rats (21 of 58) compared with control rats (3 of 63, 2 of 45, and 3 of 49 in naïve, PBS, and HK rats, respectively) (Supplementary Figs. S3 and S4, Table S2), where the subthreshold membrane potential oscillations is considered an essential requirement for the generation of abnormal spontaneous discharges that represented a primary index of neuronal hyperexcitability [2,43,75]. These results suggested that enhanced excitability in small DRG neurons appeared in bone cancer rats (for reference, see our recent publication [79]).

3.4. Decrease in expression of KCNQ2 and KCNQ3 in DRG neurons in bone cancer rats

It has been established that the KCNQ/M channel acts as a brake to regulate the AP firing and the neuronal excitability [9]. We therefore hypothesized that downregulation of the KCNQ/M channel in DRG neurons may contribute to the enhanced excitability of small DRG neurons in bone cancer rats. As expected, we found that expression of KCNQ2 and KCNQ3 in DRG neurons decreased dramatically in bone cancer rats. Immunohistochemical staining revealed that the mean optical density of both KCNQ2 and KCNQ3 decreased significantly in ipsilateral small (area <600 μm^2)-sized, medium (area 600 to 1200 μm^2)-sized, and large (area >1200 μm^2)-sized DRG neurons in MRMT-1 rats compared with naïve, PBS, and HK rats (Fig. 3, $P < .001$, n = 47 to 69 per group). In addition, Western blotting detection also demonstrated the downregulation of KCNQ2 and KCNQ3 in ipsilateral L4 and L5 DRGs in MRMT-1 rats. The optical band density of both KCNQ2 and KCNQ3 also decreased prominently in MRMT-1 rats as compared with that in naïve, PBS, and HK rats (Fig. 4, $P < .001$, n = 4/group).

3.5. Decrease in M-current density of small-sized DRG neurons in bone cancer rats

Consistent with the downregulation of KCNQ2 and KCNQ3 expression in DRG neurons in bone cancer rats, we found that the M-current density (pA/pF) of small-sized DRG neurons also decreased significantly in MRMT-1 rats (1.65 ± 0.2) in contrast to naïve (3.50 ± 0.3), PBS-treated (3.35 ± 0.4), and HK-treated (3.34 ± 0.3) rats ($P < .001$, Fig. 5A and B). Additionally, we also studied the current-voltage relationship of M currents and the concentration dependence of inhibition of M currents by XE-991 from small DRG neurons in bone cancer rats as compared with control rats. However, no significant alteration was observed in the mean instantaneous and steady-state I–V relationships for M currents among all groups (Fig. 5C and D). Coincidently, there was no obvious difference in the voltage dependence of fast and slow deactivation time constants (τ) of M currents among all groups (Fig. 5E and F). XE-991 inhibition of M current was concentration dependent (Fig. 5G). The concentration–response curves for the inhibition of M currents by XE-991 were fitted with the Hill function. No shift was observed between the two curves obtained from naïve and MRMT-1 rats (Fig. 5H). Accordantly, no alterations in the IC_{50} for inhibition of the M currents by XE-991 (naïve, 0.50 ± 0.1 μM; MRMT-1, 0.46 ± 0.1 μM, $P > .05$, unpaired t test) and the Hill coefficient (naïve, 1.4 ± 0.1; MRMT-1, 1.4 ± 0.2, $P > .05$, unpaired t test) were observed in naïve and MRMT-1 rats. These results suggested that implantation of MRMT-1 tumour cells into the tibial canal in rats caused a remarkable decrease in M-current density but neither in voltage-dependence and kinetics of M currents, nor in concentration dependence of XE-991 inhibition of M currents in small DRG neurons, implying that the reduction of M-current density was likely caused by the decrease in expression of KCNQ/M channels in MRMT-1 rat DRG neurons.

3.6. Inhibition of M currents by XE-991 enhanced the DRG neuron excitability in normal rats

In a recent study, Rose et al. [60] have reported that downregulation of the *Kcnq2* gene encoding the M channel subunit Kv7.2 by REST may contribute to the neuropathic overexcitability of peripheral sensory fibres. To further examine whether inhibition of KCNQ/M channels mediate the hyperexcitability of DRG neurons, we therefore tested the effects of XE-991, a selective KCNQ/M-channel blocker, on M currents and the firing properties of small DRG neurons (capacitance 19.1 ± 0.7 pF) evoked by a depolarizing current pulse (1-second, 2-fold AP threshold) in naïve rats. Of 19 recorded cells, 16 responded to XE-991 with a significant inhibition of M currents, whereas the remaining 3 of 19 cells showed no response (Supplementary Fig. S5). As shown in Fig. 6 and Supplementary Table S3, inhibition of M currents by XE-991 (1 μM) dramatically enhanced DRG neuron excitability manifested as an increase in AP frequency ($P < .001$) and decreases in $AHP_{80\%}$ duration ($P < .01$), the first and second AP duration ($P < .05$), and ISI ($P < .01$) of evoked APs (paired t test, n = 16). Other alterations of intrinsic electrogenic properties, including obvious depolarization of RMP and decreases in AP amplitude and overshot, were shown in Supplementary Table S3. An example of evoked APs recorded from a small DRG neuron (capacitance 18.1 pF) before and after perfusion of XE-991 (1 μM) is shown in Fig. 6B. An enlarged trace from the left panel (in the square box) is shown on the right.

3.7. Enhancement of M currents by retigabine inhibited the bone cancer–induced hyperexcitability of small DRG neurons in MRMT-1 rats

Next, we investigated whether repression of KCNQ/M channels contributed to the cancer-induced hyperexcitability of small DRG neurons in MRMT-1 rats. We examined the effects of retigabine, a selective KCNQ/M-channel opener, on M currents and the properties of APs evoked by a depolarizing current pulse (1-second, 2-fold AP threshold), recorded from small DRG neurons (capacitance 18.7 ± 0.8 pF) in bone cancer rats. Of 21 recorded cells, 15 responded to retigabine with a prominent potentiation of M currents, whereas the other 6 cells showed no response (Supplementary Fig. S5). Our results showed that enhancement of M currents by retigabine (20 μM) markedly inhibited the cancer-induced hyperexcitability of small DRG neurons manifested as a decrease in AP frequency ($P < .01$) and increases in $AHP_{80\%}$ duration ($P < .05$), the second AP duration ($P < .05$), and ISI ($P < .05$) of evoked APs (paired t test, n = 15) (Fig. 7 and Supplementary Table S3). Other alterations of intrinsic electrogenic properties including obvious hyperpolarization of RMP and increase in AP amplitude were shown in Supplementary Table S3. A representative example of evoked APs recorded from a small DRG neuron (capacitance 19.4 pF) before and after perfusion of retigabine (20 μM) is shown in Fig. 7B. An enlarged trace from the left panel (in the square box) is shown on the right.

3.8. Intraperitoneal administration of XE-991 produced mechanical allodynia in normal rats

Because the aforementioned results suggested that inhibition of M currents contributes to the hyperexcitability of small DRG neurons in bone cancer rats, we therefore hypothesized that suppression of KCNQ/M channels in small-sized DRG neurons plays a

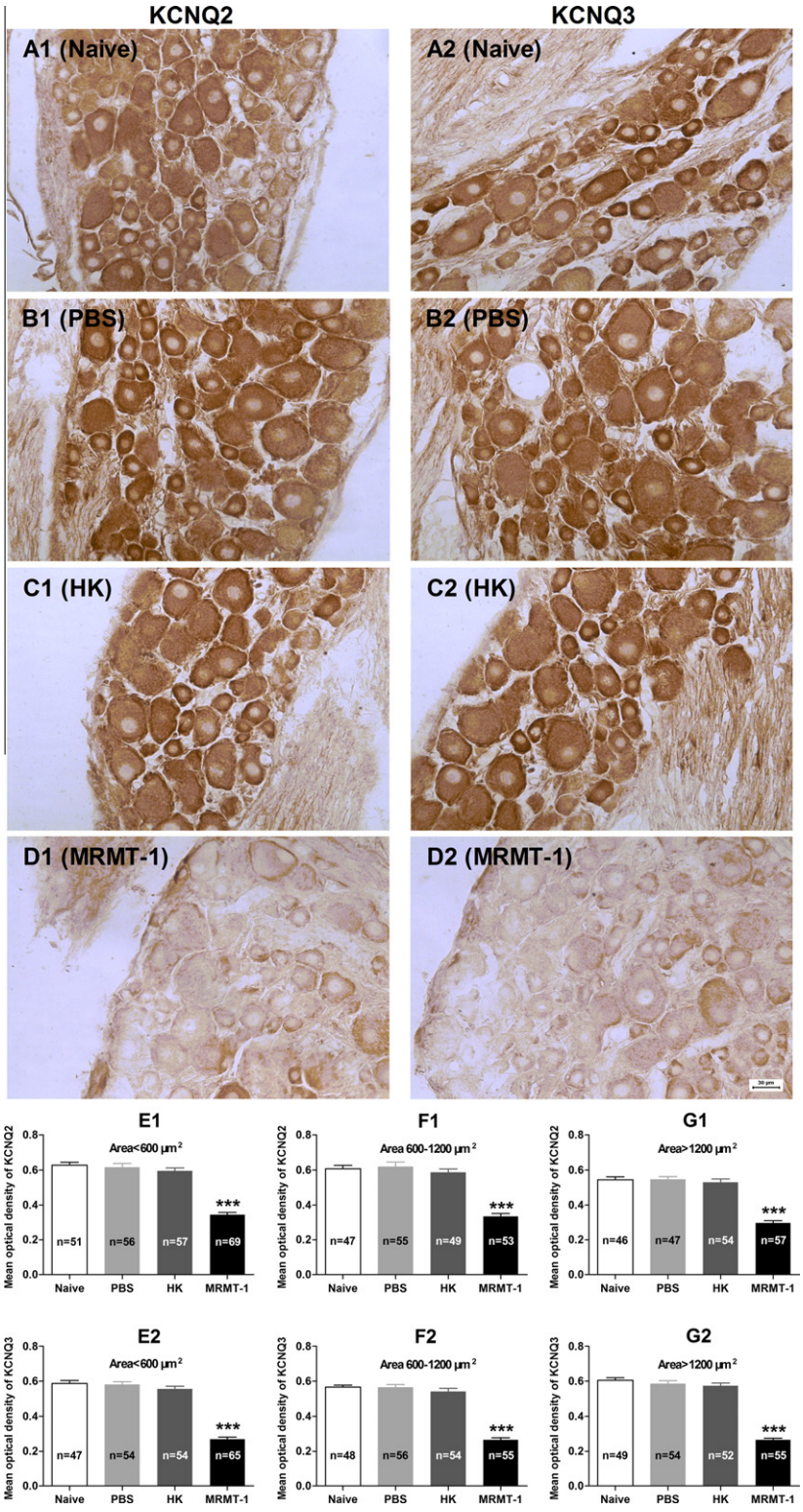

Fig. 3. Immunohistochemical staining of KCNQ2 and KCNQ3 in ipsilateral L4 and L5 dorsal root ganglia (DRG) neurons in naïve, phosphorylated buffer solution (PBS), heat-killed (HK), and MRMT-1 rats. DRG tissues were obtained on day 14 postsurgery. (A1 to D1) A representative example of KCNQ2-positive expression in DRG neurons in naïve (A1), PBS (B1), HK (C1), and MRMT-1 (D1) rats. (A2 to D2) A representative example of KCNQ3-positive expression in DRG neurons in naïve (A2), PBS (B2), HK (C2), and MRMT-1 (D2) rats. (E to G) Summary of mean integrated optical density values of KCNQ2 (E1 to G1) and KCNQ3 (E2 to G2) expression from 5 consecutive sections (80-μm interval) of each DRG from 3 animals in each group. Note that expression of both KCNQ2 and KCNQ3 decreased significantly in small-sized (area <600 μm^2), medium-sized (area 600 to 1200 μm^2), and large-sized (area >1200 μm^2) DRG neurons in MRMT-1 rats. $^{***}P < .001$, compared with naïve, PBS, or HK groups, one-way ANOVA followed by Dunnett multiple comparison test. Values are presented as mean ± SEM with the number given in each column. Scale bar = 50 μm.

crucial role in the development of bone cancer pain. Here, we first investigated the effect of intraperitoneal administration of XE-991, a selective KCNQ/M-channel blocker, on mechanical and thermal pain behaviours in normal rats. We found that inhibition of the

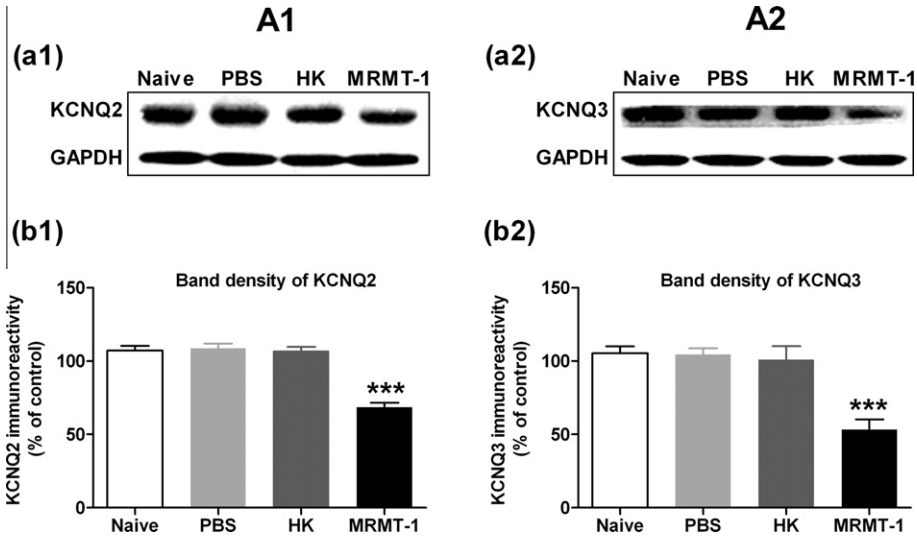

Fig. 4. Western blotting detection of KCNQ2 and KCNQ3 expression in ipsilateral L4 and L5 dorsal root ganglia (DRG) in naïve, phosphorylated buffer solution (PBS), heat-killed (HK), and MRMT-1 rats. (A1) KCNQ2. (A2) KCNQ3. (a1, a2) Western blotting bands. Upper row: KCNQ2 or KCNQ3; lower row: glyceraldehyde 3-phosphate dehydrogenase. (b1, b2) Analysis of the optical band density. Note that expression of both KCNQ2 and KCNQ3 decreased significantly in ipsilateral (left) L4 and L5 DRGs in MRMT-1 rats. $^{***}P < .001$, compared with naïve, PBS, or HK groups, one-way ANOVA followed by Dunnett multiple comparison test, n = 4 rats in each group.

KCNQ/M channel by XE-991 produced an obvious mechanical allodynia but not thermal hyperalgesia in normal rats. As shown in Fig. 8A1–8C1, XE-991 induced a significant decrease in 50% PWT to von Frey filaments in a dose-dependent manner. For example, at the dose of 0.25 mg/kg, XE-991 had no significant effect on 50% PWT at any time point after injection ($P > .05$, two-way ANOVA, Fig. 8A1). As the dose increased, XE-991 decreased the 50% PWT significantly from 0.5 to 1.0 mg/kg ($P < .001$, two-way ANOVA, Fig. 8A1), and this decreased effect was enhanced as the dose of XE-991 increased. At the dose of 1.0 mg/kg, the 50% PWT decreased markedly to 4.3 ± 0.3 *g* from the vehicle control of 14.8 ± 0.3 *g* at the 60-minute time point after XE-991 injection ($P < .001$, two-way ANOVA, Fig. 8A1 and 8C1). As summarized in the area under the time-course curve (AUC) of 50% PWT from Fig. 8A1, a similar reduction was observed at the dose of 0.5, 0.75, and 1.0 mg/kg, respectively ($P < .01$ to .001, one-way ANOVA, Fig. 8B1). Unexpectedly, no significant alteration was observed on the PWL at any dose of XE-991 application (Fig. 8A2–8C2).

3.9. Intraperitoneal administration of retigabine alleviated mechanical allodynia and thermal hyperalgesia in bone cancer rats

Finally, we investigated the effects of intraperitoneal administration of retigabine, a selective KCNQ/M-channel opener, on cancer-induced pain behaviours in MRMT-1 rats. We found that activation of the KCNQ/M channel by retigabine alleviated both mechanical allodynia and thermal hyperalgesia in bone cancer rats. As shown in Fig. 9, retigabine significantly inhibited the bone cancer–induced reduction of 50% PWT to von Frey filaments and PWL to radiant heat stimulus in a dose-dependent manner. For example, the cancer-induced reduction of 50% PWT was prominently inhibited by retigabine at the beginning dose of 4 mg/kg, and this inhibitory effect of retigabine was enhanced as the dose increased ($P < .001$, two-way ANOVA, Fig. 9A1). As summarized in the AUC of 50% PWT from Fig. 9A1, a similar inhibitory effect of retigabine was observed at the dose of 4, 6, and 8 mg/kg, respectively ($P < .01$ to .001, one-way ANOVA, Fig. 9B1). Moreover, we also found that the inhibitory effect of retigabine on the reduction of PWT in bone cancer rats was almost completely blocked by the KCNQ/M-channel antagonist XE-991 ($P < .001$, one-way ANOVA, Fig. 9C1). Similarly, retigabine also inhibited the reduction of PWL in bone cancer rats in a dose-dependent manner, and this inhibitory effect of retigabine could also be blocked by XE-991 (Fig. 9A2–9C2). These results suggested that activation of the KCNQ/M channel by retigabine alleviated both mechanical allodynia and thermal hyperalgesia in bone cancer rats, and these inhibitory effects of retigabine could be blocked by the KCNQ/M-channel antagonist XE-991.

4. Discussion

4.1. Suppression of KCNQ/M channels in cancer rat DRG neurons

Consistent with a previous report that expression of the *KCNQ2* gene encoding the Kv7.2 subunit of the M channel is markedly suppressed in rat DRGs after peripheral nerve injury [60], we here observed a remarkable decrease in expression of KCNQ2 and KCNQ3 proteins and a reduction of M-current density in MRMT-1 rat DRG neurons. In this study, we found that the magnitude of M currents is smaller than previous reports [31,53,65]. We speculated that the M currents might suffer a rundown under whole-cell patch clamp recording without additional adenosine triphosphate (ATP) in the pipette solution because the loss of membrane PIP2 in the absence of ATP could cause rundown of M currents [10]. In our experiments, we filled a patch pipette with internal solution containing K-acetate instead of high-concentration of KCl to reduce calcium-mediated rundown of M currents [69] because intracellular high KCl-induced outward chloride flux may lead to great inward calcium flux [69]. Additionally, after forming the whole-cell clamp, M currents were recorded rapidly within 3 seconds for M-current amplitude examination, 70 seconds for deactivation I–V curve analyses, and 150 seconds for application of XE-991 and retigabine, respectively. During this time window (1 to 3 minutes), the rundown of M currents was probably small because rundown is a much slower process than gating (minutes as opposed to seconds) [37,46]. Indeed, we found a small rundown rate of M currents at this time window (6.6% ± 0.8% in naïve cells and 5.5% ± 0.9% in MRMT-1 cells, n = 40/group) (Supplementary Fig. S6). Certainly, to further reduce the rundown of M currents, a perforated patch clamp recording with additional ATP in the pipette solution should be used. In a preliminary experiment, we

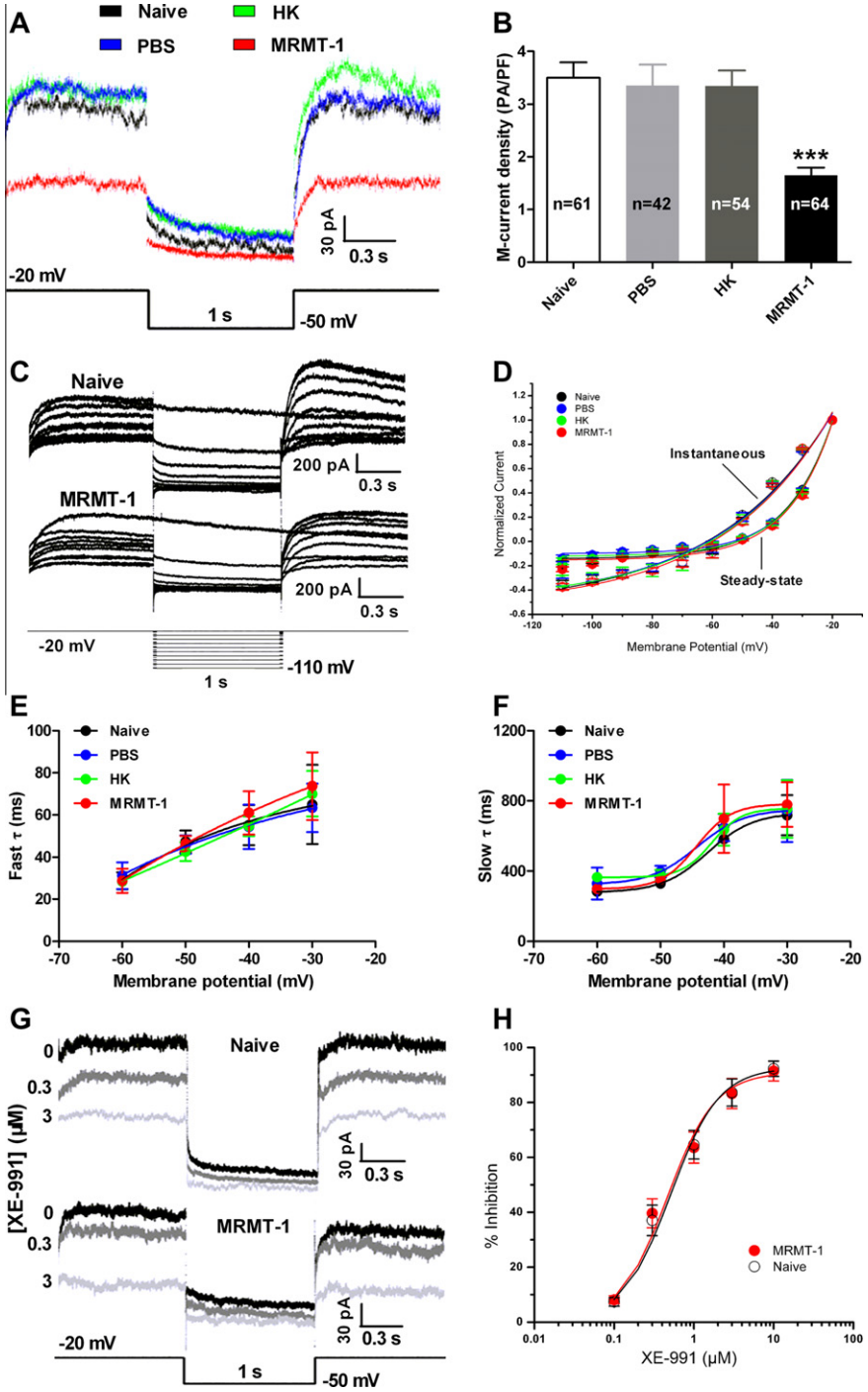

Fig. 5. Decrease in M-current density of small-sized dorsal root ganglia (DRG) neurons in bone cancer rats. (A) A representative example of M currents recorded from small DRG neurons in naïve (17.7 pF), phosphorylated buffer solution (PBS) (19.3 pF), heat-killed (HK) (16.5 pF), and MRMT-1 (17.9 pF) rats. (B) Summary of the M-current density from naïve (n = 61; capacitance 17.4 ± 0.6 pF), PBS (n = 42; capacitance 18.1 ± 0.4 pF), HK (n = 54; capacitance 17.6 ± 0.8 pF), and MRMT-1 (n = 64; capacitance 18.7 ± 0.3 pF) rat DRG neurons. The M-current density was calculated as the amplitude of M current (pA) divided by the membrane capacitance (pF) of the recorded DRG neuron, in which the amplitude of M currents was measured from deactivation current records at −50 mV as the difference between the current 10 to 20 ms after the beginning of the voltage step and the current at the end of the step. Note that the density of M currents decreased significantly in MRMT-1 rats in contrast to naïve, PBS, or HK rats. $^{***}P < .001$, compared with naïve, PBS, or HK groups, one-way ANOVA followed by Dunnett multiple comparison test. (C) A representative example of deactivation currents recorded from small DRG neurons in naïve (17.4 pF) and MRMT-1 (20.1 pF) rats. The cells were held at −20 mV to generate sustained outward currents. The channels were then deactivated by applying a 1-second hyperpolarizing pulse from −20 mV to −110 mV in increments of −10 mV every 4 seconds. (D) Mean instantaneous and steady-state I–V relationships for M currents recorded from small DRG neurons (capacitance 18.2 ± 0.7, 18.2 ± 1.0, 18.3 ± 0.7, and 17.9 ± 0.6 pF in naïve, PBS, HK, and MRMT-1 rats), obtained by measuring the current at the beginning and the end of the voltage pulse, respectively. Note that both of them did not change among all groups ($P > .05$, two-way ANOVA; n = 11 to 12/group). (E, F) Plots of the voltage dependence of fast (E) and slow (F) deactivation time constants (τ) of M currents recorded from small DRG neurons in naïve (capacitance 18.2 ± 0.9 pF), PBS (capacitance 18.1 ± 1.0 pF), HK (capacitance 17.9 ± 0.8 pF), and MRMT-1 (capacitance 17.9 ± 0.7 pF) rats. Data points were fitted with a Boltzmann equation. Note that there was no difference in the voltage dependence of fast and slow deactivation time constants (τ) of M currents among all groups ($P > .05$, two-way ANOVA; n = 11 to 12/group). (G, H) Inhibition of M currents by XE-991 (0.1 to 10 μM). (G) A representative example of the M current curves in the presence of XE-991 at 0, 0.3, and 3 μM recorded from small DRG neurons in naïve (19.4 pF) and MRMT-1 (19.8 pF) rats. XE-991 inhibition of the M current was concentration dependent. Note the shift in the baseline outward current in XE-991 (at holding potential of −20 mV). (H) Concentration–response curves for the inhibition of M currents by XE-991 in naïve (black, n = 10) and MRMT-1 (red, n = 8) rats. The curves were fitted with Hill function. No shift was observed between the two curves.

actually recorded larger M currents with additional ATP in the pipette solution even though under whole-cell patch clamp recording (Supplementary Fig. S7).

Mechanisms underlying the repression of KCNQ/M channels in MRMT-1 rat DRG neurons were not further studied. We hypothesized that the transcriptional downregulation of *KCNQ* gene expression by REST (repressor element 1-silencing transcription factor), which has been previously identified in vitro [49] and in a rat model of neuropathic pain [60], might contribute to the reduction of KCNQ/M channels in MRMT-1 rat DRG neurons. Indeed, we observed a strong downregulation of KCNQ2 and KCNQ3 mRNA levels accompanying an obvious increase in the mRNA level of REST in cancer rat DRGs (unpublished data). Certainly, we cannot exclude other indirect mechanisms such as calmodulin-mediated Ca^{2+}-dependent regulation of KCNQ/M-channel trafficking and function [4,18,21]; membrane PtdIns(4,5)P2 hydrolysis and channel phosphorylation by many neurotransmitters through their G-protein-coupled receptors [22,31,32,40,76,77], which are now well considered as two pathways of KCNQ/M-channel modulation [8,13,28]. Altogether, we demonstrated for the first time to our knowledge that implantation of MRMT-1 tumour cells produced marked decreases in expression and function of KCNQ2 and KCNQ3 channels, suggesting a suppression of KCNQ/M channels in cancer rat DRG neurons.

4.2. Suppression of KCNQ/M channels contributes to the hyperexcitability of cancer rat DRG neurons

Consistent with literature findings that modulation of KCNQ/M channels has an important impact on neuronal excitability [9,12,20,53,54,64], we observed that inhibition of the KCNQ/M channel with XE-991 caused a robust increase in the excitability of naive rat DRG neurons, whereas activation of the KCNQ/M channels with retigabine significantly inhibited the hyperexcitability of MRMT-1 rat DRG neurons, and all of the effects of retigabine could be reversed by the KCNQ/M-channel blocker XE-991. We cannot give a precise explanation for our intricate finding that retigabine can still reduce the hyperexcitability of MRMT-1 rat DRG neurons, even though the M-current density is greatly reduced. It is suggested that the membrane potential in sympathetic and sensory neurons can be set by a dynamic equilibrium of two opposing currents, depolarizing I_h (hyperpolarization-activated current conducted by HCN channels) and hyperpolarizing I_M; with I_h being activated at the potentials negative to −50 mV and I_M activating at potentials positive to −60 mV [1,38]. Thus, when M-channel abundance is decreased and the neuron is tonically depolarized, activation of residual M channels results in reversion of depolarization back to the level at which I_h starts coming into play, which results in a reset of an overexcitable neuron into a normal excitability state [60]. We therefore propose that although the M-channel

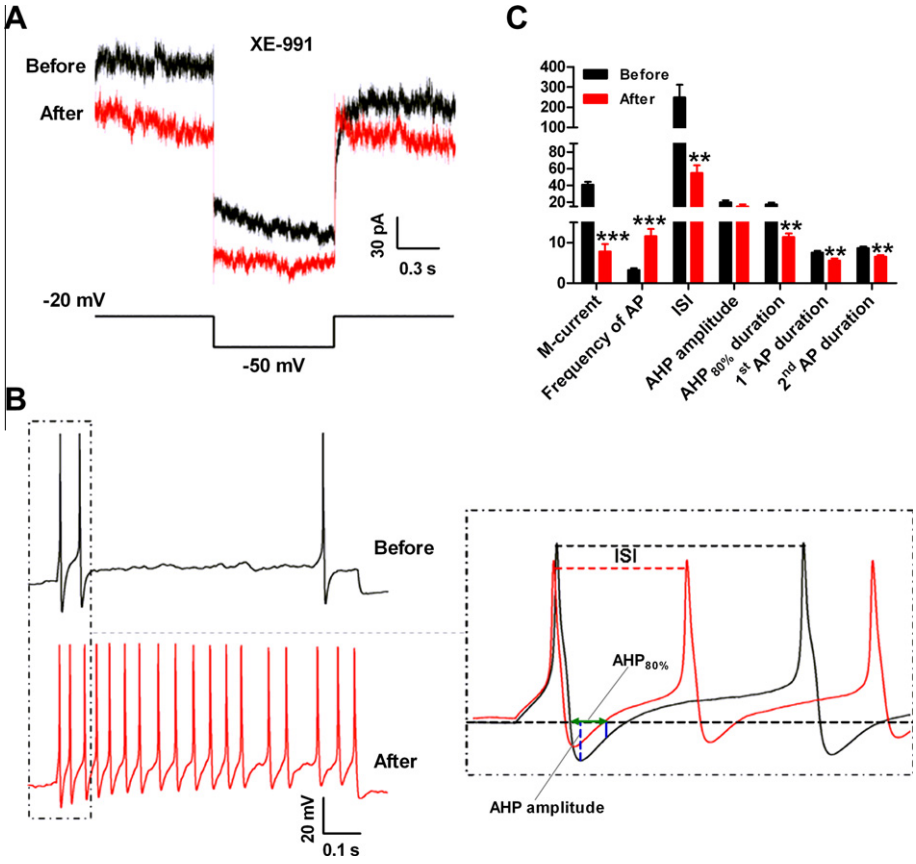

Fig. 6. Effects of XE-991, a selective KCNQ/M channel blocker, on M currents and the properties of action potentials (APs) evoked by a depolarizing current pulse (1-second, 2-fold AP threshold), recorded from small dorsal root ganglia (DRG) neurons in naïve rats. (A) A representative example of M currents recorded from a small DRG neuron (18.1 pF) before and after perfusion of XE-991 (1 μM). (B) A representative example of evoked APs recorded from the same DRG neuron before and after perfusion of XE-991 (1 μM). Enlarged trace from left panel (in the square box) is shown on the right. (C) Summary of M currents and the properties of evoked APs from 16 responded DRG neurons (capacitance 19.4 ± 0.8 pF) before and after perfusion of XE-991 (1 μM). $^{**}P < .01$, $^{***}P < .001$, before vs after, paired *t* test. Note that inhibition of M currents by XE-991 dramatically enhanced the DRG neuron excitability manifested as an increase in AP frequency and decreases in $AHP_{80\%}$ duration, the second AP duration, and interspike intervals. $AHP_{80\%}$ duration: after hyperpolarization duration at 80% repolarization.

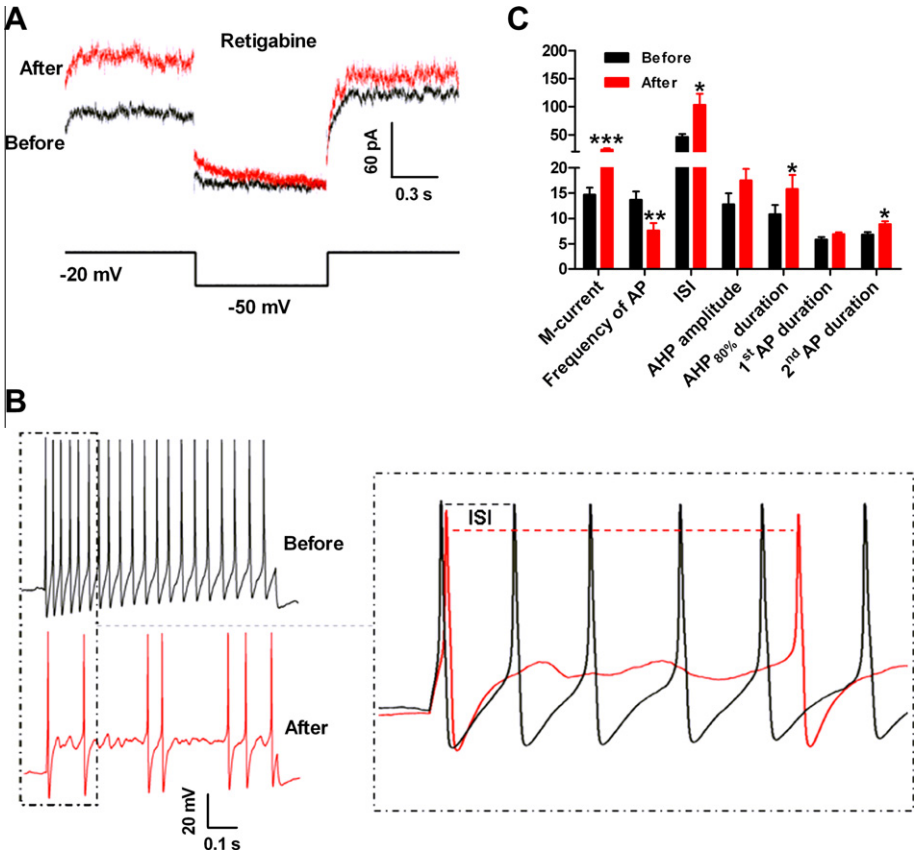

Fig. 7. Effects of retigabine, a selective KCNQ/M channel opener, on M currents and the properties of action potentials (APs) evoked by a depolarizing current pulse (1-second, 2-fold AP threshold), recorded from small dorsal root ganglia (DRG) neurons in bone cancer rats. (A) A representative example of M currents recorded from a small DRG neuron (18.1 pF) of MRMT-1 rat before and after perfusion of retigabine (20 μM). (B) A representative example of evoked APs recorded from the same DRG neuron before and after perfusion of retigabine (20 μM). Enlarged trace from the left panel (in the square box) is shown in the right. (C) Summary of M currents and the properties of evoked APs from 15 responded DRG neurons (capacitance 18.6 ± 0.6 pF) before and after perfusion of retigabine (20 μM). $^{*}P < .05$, $^{**}P < .01$, before vs after, paired *t* test. Note that enhancement of M currents by retigabine markedly inhibited the cancer-induced hyperexcitability of small DRG neurons manifested as a decrease in AP frequency and increases in $AHP_{80\%}$ duration, the second AP duration, and interspike intervals of evoked APs.

expression and the M-current density are significantly decreased in MRMT-1 rat DRG neurons, the residual M channels on DRG neurons can still be activated by retigabine [52], which will hyperpolarize the neurons and reduce the neuronal excitability [9,41,53,66]. Taken together, our present results provide strong evidence for the notion that the KCNQ/M channel can be regarded as a device to both stabilize the neuronal resting potential and constrain overexcitability by regulating the AP threshold [9]; therefore, suppression of the KCNQ/M channel likely underlies the hyperexcitability of primary DRG neurons in bone cancer rats.

4.3. Suppression of KCNQ/M channels in DRG neurons contributes to the development of bone cancer pain

We herein provided direct evidence that suppression of KCNQ/M channels in DRG neurons plays a crucial role in bone cancer pain. We found that activation of the KCNQ/M channel with retigabine alleviated both mechanical allodynia and thermal hyperalgesia in bone cancer rats, whereas suppression of the channel with XE-991 produced an obvious mechanical allodynia in naive rats. We cannot give a clear explanation regarding why XE-991 induced mechanical allodynia but not thermal hyperalgesia in naive rats, whereas retigabine inhibited both of them in MRMT-1 rats. More recently, Passmore et al. [52] have shown that the role of M channels in A-δ fibres seems quite functionally distinct from the role in C-fibres. Under the physiological state, M channels are active at or near the resting potential in myelinated A-β and A-δ mechanosensitive fibre terminals but are not very active in heat-sensitive C-fibre terminals [52]. Thus, XE-991 preferentially blocks those activated M channels located at the myelinated A-β and A-δ fibre terminals (mainly sensitive to mechanical stimuli) but has little effect on inactivated M channels located at the unmyelinated C-fibre terminals (mainly sensitive to noxious heat stimuli). Consequently, XE-991 potentiated mechanical but not thermal responses in naive rats. On the contrary, as an M-channel enhancer, retigabine has a facilitating effect on both active and not very active M channel [41]. It has been validated that retigabine can produce a hyperpolarizing shift in the activation curve for M channel [66]. Accordingly, as long as M channels were present, whether or not they were normally very active at rest, they would be activated, and would produce a large hyperpolarization and increase in the conductance shunt in the presence of retigabine [52]. Therefore, retigabine will likely activate the M channels located at both the myelinated A-β and A-δ fibre terminals and the unmyelinated C-fibre terminals, and reduce their excitability that underlie the mechanical and thermal nociceptive responses. In support of this notion, we actually observed a mixed population of A-δ-type and C-type DRG neurons in our cultures as assessed by their electrophysiological baseline properties (Supplementary Fig. S8 and Supplementary Table S4) [16,19]. Together with our electrophysiological data showing that inhibition of the KCNQ/M channel with XE-991 dramatically enhanced DRG neuron excitability in normal rats, whereas enhancement of M currents with retigabine markedly inhibited the hyperexcitability of MRMT-1 DRG neurons, we

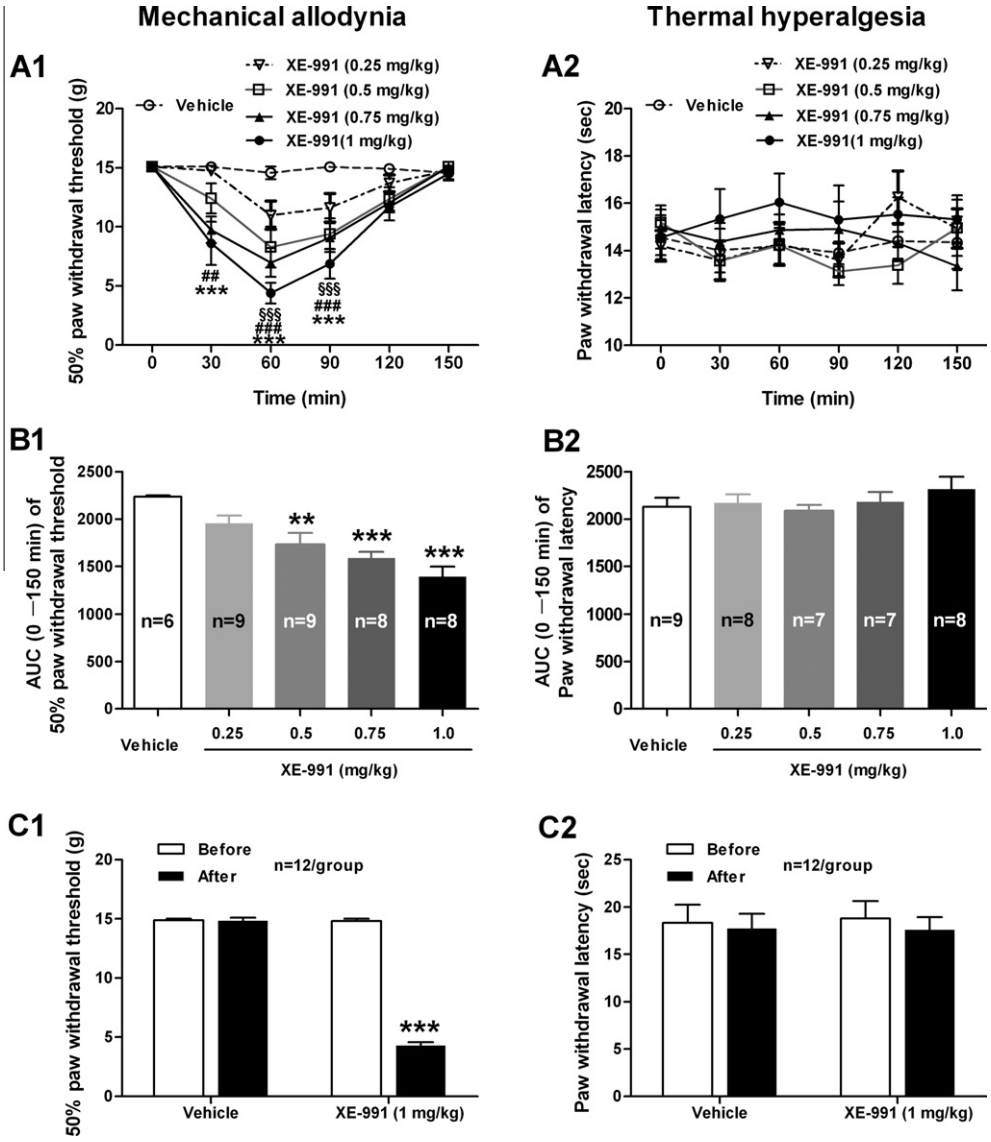

Fig. 8. Intraperitoneal administration of XE-991 produced mechanical allodynia but not thermal hyperalgesia in normal rats. (A1, A2) Effects of XE-991 at 0.25, 0.5, 0.75, and 1.0 mg/kg body weight on mechanical (A1) and thermal (A2) pain behaviours. Note that XE-991 significantly decreased the 50% paw withdrawal threshold (PWT) to von Frey filaments at various doses. No significant alteration was observed on paw withdrawal latency (PWL) to radiant heat, $^{§§§}P < .001$ (0.5 mg/kg), $^{\#\#}P < .01$ (0.75 mg/kg), $^{\#\#\#}P < .001$ (0.75 mg/kg), $^{***}P < .001$ (1 mg/kg), compared with vehicle group, two-way ANOVA followed by Bonferroni post hoc test, n = 6 to 9/group. (B1, B2) Area under the time-course curve (AUC) of 50% PWT and PWL in (A1) and (A2), respectively. $^{**}P < .01$, $^{***}P < .001$, compared with vehicle group, one-way ANOVA followed by Dunnett multiple comparison test, values are presented as mean ± SEM with the number given in each column. (C1, C2) Effects of XE-991 (1 mg/kg) on 50% PWT (C1) and PWL (C2) as measured at 60 minutes after drug administration. $^{***}P < .001$, before vs after, two-way ANOVA followed by Bonferroni multiple comparison test, n = 12/group.

suggest that repression of KCNQ/M channels leads to the hyperexcitability of primary sensory neurons, which in turn causes the development of bone cancer pain.

Certainly, because M-current modulators are given systemically in our behavioural experiments, we cannot rule out the possibility that retigabine can cross the blood–brain barrier and act at sites other than DRG neurons. Indeed, in the dorsal spinal cord, retigabine exerts a strong depressant effect on the delayed sensitization of dorsal horn neurons reflected in the recordings of windup [53]. Moreover, retigabine has been found to reduce the transmission of Aδ-fibre and C-fibre responses into the spinal dorsal horn [53] and hyperpolarizes the primary afferent fibres [57]. It is suggested that the most common effects of retigabine in central neurons are hyperpolarization and spike frequency adaptation as a consequence of M-current facilitation [59]. Additionally, retigabine applied at neuroma endings of axotomized fibres produces a hyperpolarization and a reduction of the excitability in aberrant sensory endings [61]. It is proposed that this effect of retigabine is most likely mediated by the opening KCNQ/M channels accumulated at axotomized endings [3,61]. Taking these data together with our present findings, we suggest that KCNQ/M currents contribute to modulate the excitability of DRG neurons [53], the dorsal horn neurons in the spinal cord [56], the central projections from primary afferents [57], and the site of injury [61]. In these sensory elements, enhancement of KCNQ/M current by the application of retigabine evoked a hyperpolarizing effect that underlies the antihyperalgesic activity of retigabine in animal models of chronic pain [5,17,53].

In conclusion, our present study suggests that implantation of MRMT-1 tumour cells into the tibial canal in rats produces a prominent repression of KCNQ/M channels in primary DRG neurons, which may underlie the hyperexcitability of these DRG neurons as well as mechanical allodynia and thermal hyperalgesia in bone cancer rats. Thus, suppression of KCNQ/M channels in primary sensory neurons plays a vital role in bone cancer pain.

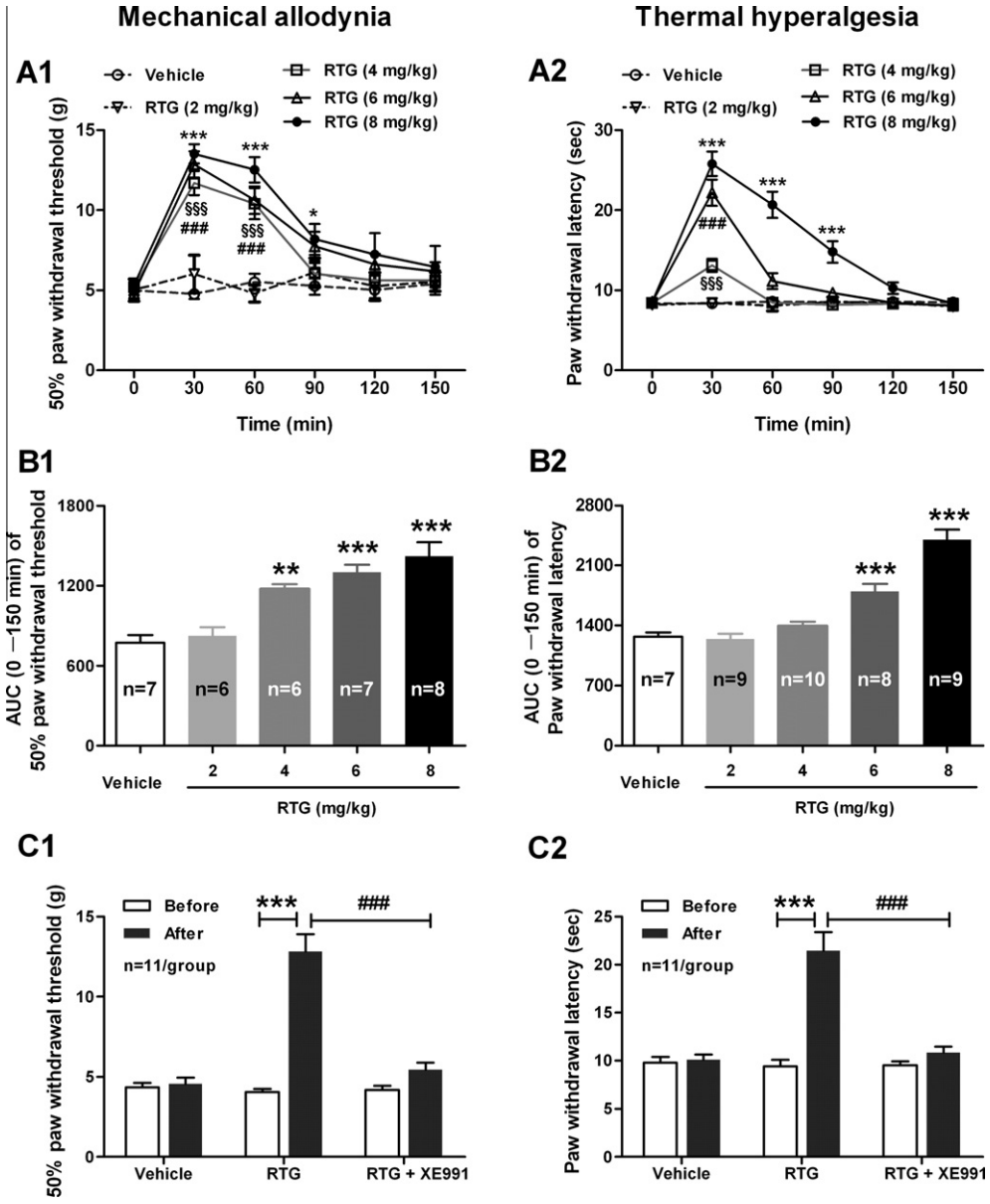

Fig. 9. Intraperitoneal administration of retigabine (RTG) alleviated mechanical allodynia and thermal hyperalgesia in bone cancer rats. (A1, A2) Effects of retigabine (2, 4, 6, and 8 mg/kg) on mechanical (A1) and thermal (A2) pain behaviours in rats measured on day 14 after inoculation of MRMT-1 tumour cells. Note that retigabine significantly inhibited the bone cancer–induced reduction of 50% PWT to von Frey filaments and PWL to radiant heat, $^{§§§}P < .001$ (4 mg/kg), $^{###}P < .001$ (6 mg/kg), $^{*}P < .05$, $^{***}P < .001$ (8 mg/kg), compared with vehicle group, two-way ANOVA followed by Bonferroni post hoc test, n = 6 to 10/group. (B1, B2) AUC of 50% PWT and PWL in (A1) and (A2). $^{**}P < .01$, $^{***}P < .001$, compared with vehicle group, one-way ANOVA followed by Dunnett multiple comparison test, values are presented as mean ± SEM with the number given in each column. (C1, C2) Effects of retigabine (8 mg/kg) and retigabine (8 mg/kg) plus XE-991 (1 mg/kg) on 50% PWT (C1) and PWL (C2) in bone cancer rats as measured at 30 minutes after drug administration. Note that retigabine significantly reversed both the bone cancer–induced reduction of PWT to von Frey filaments and PWL to radiant heat, and these effects of retigabine were obviously blocked by XE-991. $^{***}P < .001$, before RTG vs after RTG; $^{###}P < .001$, after RTG vs after RTG + XE-991, two-way ANOVA followed by Bonferroni multiple comparison test, n = 11/group.

Acknowledgements

The present work was supported by grants from the National Natural Science Foundation of China (31171063, 81072951, 61027001), the Beijing Natural Science Foundation (7112079), the special foundation for public welfare profession scientific research program from Ministry of Health of the Peoples Republic of China (201302013), and the 973 Program of the Ministry of Science and Technology of China (2013CB531905). The authors have no conflicts of interest to declare.

Appendix A. Supplementary data

Supplementary data associated with this article can be found, in the online version, at http://dx.doi.org/10.1016/j.pain.2012.12.005.

References

[1] Akasu T, Tokimasa T. Cellular metabolism regulating hours and M currents in bullfrog sympathetic ganglia. Can J Physiol Pharmacol 1992;70:S51–5.
[2] Amir R, Michaelis M, Devor M. Membrane potential oscillations in dorsal root ganglion neurons: role in normal electrogenesis and neuropathic pain. J Neurosci 1999;19:8589–96.

[3] Arroyo EJ, Sirkowski EE, Chitale R, Scherer SS. Acute demyelination disrupts the molecular organization of peripheral nervous system nodes. J Comp Neurol 2004;479:424–34.
[4] Bal M, Zhang J, Hernandez CC, Zaika O, Shapiro MS. Ca^{2+}/calmodulin disrupts AKAP79/150 interactions with KCNQ (M Type) K^+ channels. J Neurosci 2010;30:2311–23.
[5] Bi Y, Chen H, Su J, Cao X, Bian X, Wang K. Visceral hyperalgesia induced by forebrain-specific suppression of native Kv7/KCNQ/M current in mice. Mol Pain 2011;7:84–97.
[6] Biervert C, Schroeder BC, Kubisch C, Berkovic SF, Propping P, Jentsch TJ, Steinlein OK. A potassium channel mutation in neonatal human epilepsy. Science 1998;279:403–6.
[7] Blackburn-Munro G, Jensen BS. The anticonvulsant retigabine attenuates nociceptive behaviours in rat models of persistent and neuropathic pain. Eur J Pharmacol 2003;460:109–16.
[8] Brown DA, Hughes SA, Marsh SJ, Tinker A. Regulation of M(Kv7.2/7.3) channels in neurons by PIP(2) and products of PIP(2) hydrolysis: significance for receptor-mediated inhibition. J Physiol 2007;582:917–25.
[9] Brown DA, Passmore GM. Neural KCNQ (Kv7) channels. Br J Pharmacol 2009;156:1185–95.
[10] Chambard JM, Ashmore JF. Regulation of the voltage-gated potassium channel KCNQ4 in the auditory pathway. Pflugers Arch 2005;450:34–44.
[11] Chaplan SR, Bach FW, Pogrel JW, Chung JM, Yaksh TL. Quantitative assessment of tactile allodynia in the rat paw. J Neurosci Methods 1994;53:55–63.
[12] Crozier RA, Ajit SK, Kaftan EJ, Pausch MH. MrgD activation inhibits KCNQ/M currents and contributes to enhanced neuronal excitability. J Neurosci 2007;27:4492–6.
[13] Delmas P, Brown DA. Pathways modulating neural KCNQ/M (Kv7) potassium channels. Nat Rev Neurosci 2005;6:850–62.
[14] Devaux JJ, Kleopa KA, Cooper EC, Scherer SS. KCNQ2 is a nodal K^+ channel. J Neurosci 2004;24:1236–44.
[15] Dixon WJ. Efficient analysis of experimental observations. Annu Rev Pharmacol Toxicol 1980;20:441–62.
[16] Djouhri L, Bleazard L, Lawson SN. Association of somatic AP shape with sensory receptive properties in guinea-pig dorsal root ganglion neurones. J Physiol 1998;513:857–72.
[17] Dost R, Rostock A, Rundfeldt C. The anti-hyperalgesic activity of retigabine is mediated by KCNQ potassium channel activation. Naunyn Schmiedebergs Arch Pharmacol 2004;369:382–90.
[18] Etxeberria A, Aivar P, Rodriguez-Alfaro JA, Alaimo A, Villace P, Gomez-Posada JC, Areso P, Villarroel A. Calmodulin regulates the trafficking of KCNQ2 potassium channels. FASEB J 2008;22:1135–43.
[19] Fang X, McMullan S, Lawson SN, Djouhri L. Electrophysiological differences between nociceptive and non-nociceptive dorsal root ganglion neurones in the rat in vivo. J Physiol 2005;565:927–43.
[20] Fritch PC, Naughton-Smith G, Amato GS, Burns JF, Eargle CW, Roeloffs R, Harrison W, Jones L, Wickenden AD. Novel KCNQ2/Q3 agonists as potential therapeutics for epilepsy and neuropathic pain. J Med Chem 2010;53: 887–96.
[21] Gamper N, Shapiro MS. Calmodulin mediates Ca^{2+}-dependent modulation of M type K^+ channels. J Gen Physiol 2003;122:17–31.
[22] Gamper N, Stockand JD, Shapiro MS. Subunit-specific modulation of KCNQ potassium channels by Src tyrosine kinase. J Neurosci 2003;23:84–95.
[23] Geng SJ, Liao FF, Dang WH, Ding X, Liu XD, Cai J, Han JS, Wan Y, Xing GG. Contribution of the spinal cord BDNF to the development of neuropathic pain by activation of the NR2B-containing NMDA receptors in rats with spinal nerve ligation. Exp Neurol 2010;222:256–66.
[24] Gu N, Vervaeke K, Hu H, Storm JF. Kv7/KCNQ/M and HCN/h, but not KCa2/SK channels, contribute to the somatic medium after-hyperpolarization and excitability control in CA1 hippocampal pyramidal cells. J Physiol 2005; 566:689–715.
[25] Hamamoto DT, Khasabov SG, Cain DM, Simone DA. Tumour-evoked sensitization of C nociceptors: a role for endothelin. J Neurophysiol 2008; 100:2300–11.
[26] Hansen HH, Andreasen JT, Weikop P, Mirza N, Scheel-Kruger J, Mikkelsen JD. The neuronal KCNQ channel opener retigabine inhibits locomotor activity and reduces forebrain excitatory responses to the psychostimulants cocaine, methylphenidate and phencyclidine. Eur J Pharmacol 2007;570:77–88.
[27] Hansen HH, Ebbesen C, Mathiesen C, Weikop P, Ronn LC, Waroux O, Scuvee-Moreau J, Seutin V, Mikkelsen JD. The KCNQ channel opener retigabine inhibits the activity of mesencephalic dopaminergic systems of the rat. J Pharmacol Exp Ther 2006;318:1006–19.
[28] Hernandez CC, Zaika O, Tolstykh GP, Shapiro MS. Regulation of neural KCNQ channels: signalling pathways, structural motifs and functional implications. J Physiol 2008;586:1811–21.
[29] Hirano K, Kuratani K, Fujiyoshi M, Tashiro N, Hayashi E, Kinoshita M. Kv7.2-7.5 voltage-gated potassium channel (KCNQ2-5) opener, retigabine, reduces capsaicin-induced visceral pain in mice. Neurosci Lett 2007;413:159–62.
[30] Huang ZJ, Song XJ. Differing alterations of sodium currents in small dorsal root ganglion neurons after ganglion compression and peripheral nerve injury. Mol Pain 2008;4:20.
[31] Jia Q, Jia Z, Zhao Z, Liu B, Liang H, Zhang H. Activation of epidermal growth factor receptor inhibits KCNQ2/3 current through two distinct pathways: membrane PtdIns(4,5)P2 hydrolysis and channel phosphorylation. J Neurosci 2007;27:2503–12.
[32] Jia Z, Bei J, Rodat-Despoix L, Liu B, Jia Q, Delmas P, Zhang H. NGF inhibits M/KCNQ currents and selectively alters neuronal excitability in subsets of sympathetic neurons depending on their M/KCNQ current background. J Gen Physiol 2008;131:575–87.
[33] Jimenez-Andrade JM, Mantyh WG, Bloom AP, Ferng AS, Geffre CP, Mantyh PW. Bone cancer pain. Ann NY Acad Sci 2010;1198:173–81.
[34] Khasabov SG, Hamamoto DT, Harding-Rose C, Simone DA. Tumour-evoked hyperalgesia and sensitization of nociceptive dorsal horn neurons in a murine model of cancer pain. Brain Res 2007;1180:7–19.
[35] Klinger F, Gould G, Boehm S, Shapiro MS. Distribution of M channel subunits KCNQ2 and KCNQ3 in rat hippocampus. Neuroimage 2011;58:761–9.
[36] Knopp KL, Nisenbaum ES, Arneric SP. Evolving cancer pain treatments: rational approaches to improve the quality of life for cancer patients. Curr Pharm Biotechnol 2011;12:1627–43.
[37] Lam HD, Lemay AM, Briggs MM, Yung M, Hill CE. Modulation of Kir4.2 rectification properties and pHi-sensitive rundown by association with Kir5.1. Biochim Biophys Acta 2006;1758:1837–45.
[38] Lamas JA, Reboreda A, Codesido V. Ionic basis of the resting membrane potential in cultured rat sympathetic neurons. Neuroreport 2002;13:585–91.
[39] Lang PM, Fleckenstein J, Passmore GM, Brown DA, Grafe P. Retigabine reduces the excitability of unmyelinated peripheral human axons. Neuropharmacology 2008;54:1271–8.
[40] Li Y, Langlais P, Gamper N, Liu F, Shapiro MS. Dual phosphorylations underlie modulation of unitary KCNQ K(+) channels by Src tyrosine kinase. J Biol Chem 2004;279:45399–407.
[41] Linley JE, Pettinger L, Huang D, Gamper N. M channel enhancers and physiological M channel block. J Physiol 2012;590:793–807.
[42] Linley JE, Rose K, Patil M, Robertson B, Akopian AN, Gamper N. Inhibition of M current in sensory neurons by exogenous proteases: a signaling pathway mediating inflammatory nociception. J Neurosci 2008;28:11240–9.
[43] Liu CN, Michaelis M, Amir R, Devor M. Spinal nerve injury enhances subthreshold membrane potential oscillations in DRG neurons: relation to neuropathic pain. J Neurophysiol 2000;84:205–15.
[44] Luger NM, Mach DB, Sevcik MA, Mantyh PW. Bone cancer pain: from model to mechanism to therapy. J Pain Symptom Manage 2005;29:S32–46.
[45] Marrion NV. Control of M current. Annu Rev Physiol 1997;59:483–504.
[46] Marty A, Neher E. Potassium channels in cultured bovine adrenal chromaffin cells. J Physiol 1985;367:117–41.
[47] Medhurst SJ, Walker K, Bowes M, Kidd BL, Glatt M, Muller M, Hattenberger M, Vaxelaire J, O'Reilly T, Wotherspoon G, Winter J, Green J, Urban L. A rat model of bone cancer pain. PAIN® 2002;96:129–40.
[48] Middlemiss T, Laird BJ, Fallon MT. Mechanisms of cancer-induced bone pain. Clin Oncol (R Coll Radiol) 2011;23:387–92.
[49] Mucha M, Ooi L, Linley JE, Mordaka P, Dalle C, Robertson B, Gamper N, Wood IC. Transcriptional control of KCNQ channel genes and the regulation of neuronal excitability. J Neurosci 2010;30:13235–45.
[50] Munro G, Dalby-Brown W. Kv7 (KCNQ) channel modulators and neuropathic pain. J Med Chem 2007;50:2576–82.
[51] Paice JA, Ferrell B. The management of cancer pain. CA Cancer J Clin 2011;61:157–82.
[52] Passmore GM, Reilly JM, Thakur M, Keasberry VN, Marsh SJ, Dickenson AH, Brown DA. Functional significance of M type potassium channels in nociceptive cutaneous sensory endings. Front Mol Neurosci 2012;5:63–74.
[53] Passmore GM, Selyanko AA, Mistry M, Al-Qatari M, Marsh SJ, Matthews EA, Dickenson AH, Brown TA, Burbidge SA, Main M, Brown DA. KCNQ/M currents in sensory neurons: significance for pain therapy. J Neurosci 2003;23: 7227–36.
[54] Peretz A, Sheinin A, Yue C, Gani-Katzav N, Gibor G, Nachman R, Gopin A, Tam E, Shabat D, Yaari Y, Attali B. Pre- and postsynaptic activation of M channels by a novel opener dampens neuronal firing and transmitter release. J Neurophysiol 2007;97:283–95.
[55] Qu XX, Cai J, Li MJ, Chi YN, Liao FF, Liu FY, Wan Y, Han JS, Xing GG. Role of the spinal cord NR2B-containing NMDA receptors in the development of neuropathic pain. Exp Neurol 2009;215:298–307.
[56] Rivera-Arconada I, Lopez-Garcia JA. Effects of M current modulators on the excitability of immature rat spinal sensory and motor neurones. Eur J Neurosci 2005;22:3091–8.
[57] Rivera-Arconada I, Lopez-Garcia JA. Retigabine-induced population primary afferent hyperpolarisation in vitro. Neuropharmacology 2006;51:756–63.
[58] Rivera-Arconada I, Martinez-Gomez J, Lopez-Garcia JA. M current modulators alter rat spinal nociceptive transmission: an electrophysiological study in vitro. Neuropharmacology 2004;46:598–606.
[59] Rivera-Arconada I, Roza C, Lopez-Garcia JA. Enhancing m currents: a way out for neuropathic pain? Front Mol Neurosci 2009;2:10.
[60] Rose K, Ooi L, Dalle C, Robertson B, Wood IC, Gamper N. Transcriptional repression of the M channel subunit Kv7.2 in chronic nerve injury. PAIN® 2011;152:742–54.
[61] Roza C, Lopez-Garcia JA. Retigabine, the specific KCNQ channel opener, blocks ectopic discharges in axotomized sensory fibres. PAIN® 2008;138:537–45.
[62] Saganich MJ, Machado E, Rudy B. Differential expression of genes encoding subthreshold-operating voltage-gated K^+ channels in brain. J Neurosci 2001;21:4609–24.
[63] Sevcik MA, Ghilardi JR, Halvorson KG, Lindsay TH, Kubota K, Mantyh PW. Analgesic efficacy of bradykinin B1 antagonists in a murine bone cancer pain model. J Pain 2005;6:771–5.

[64] Shen W, Hamilton SE, Nathanson NM, Surmeier DJ. Cholinergic suppression of KCNQ channel currents enhances excitability of striatal medium spiny neurons. J Neurosci 2005;25:7449–58.
[65] Suh BC, Hille B. Recovery from muscarinic modulation of M current channels requires phosphatidylinositol 4,5-bisphosphate synthesis. Neuron 2002;35: 507–20.
[66] Tatulian L, Delmas P, Abogadie FC, Brown DA. Activation of expressed KCNQ potassium currents and native neuronal M type potassium currents by the anti-convulsant drug retigabine. J Neurosci 2001;21:5535–45.
[67] Urch C. The pathophysiology of cancer-induced bone pain: current understanding. Palliat Med 2004;18:267–74.
[68] Urch CE, Donovan-Rodriguez T, Dickenson AH. Alterations in dorsal horn neurones in a rat model of cancer-induced bone pain. PAIN® 2003; 106:347–56.
[69] Vernino S, Amador M, Luetje CW, Patrick J, Dani JA. Calcium modulation and high calcium permeability of neuronal nicotinic acetylcholine receptors. Neuron 1992;8:127–34.
[70] von Gunten CF. Pathophysiology of pain in cancer. J Pediatr Hematol Oncol 2011;33:S12–8.
[71] Wang HS, Pan Z, Shi W, Brown BS, Wymore RS, Cohen IS, Dixon JE, McKinnon D. KCNQ2 and KCNQ3 potassium channel subunits: molecular correlates of the M channel. Science 1998;282:1890–3.
[72] Wickenden AD, Naughton-Smith G. Kv7 channels as targets for the treatment of pain. Curr Pharm Des 2009;15:1773–98.
[73] Wladyka CL, Kunze DL. KCNQ/M currents contribute to the resting membrane potential in rat visceral sensory neurons. J Physiol 2006;575:175–89.
[74] Wulff H, Castle NA, Pardo LA. Voltage-gated potassium channels as therapeutic targets. Nat Rev Drug Discov 2009;8:982–1001.
[75] Xing JL, Hu SJ, Long KP. Subthreshold membrane potential oscillations of type A neurons in injured DRG. Brain Res 2001;901:128–36.
[76] Zaika O, Lara LS, Gamper N, Hilgemann DW, Jaffe DB, Shapiro MS. Angiotensin II regulates neuronal excitability via phosphatidylinositol 4,5-bisphosphate-dependent modulation of Kv7 (M type) K^+ channels. J Physiol 2006;575:49–67.
[77] Zhang H, Craciun LC, Mirshahi T, Rohacs T, Lopes CM, Jin T, Logothetis DE. PIP(2) activates KCNQ channels, and its hydrolysis underlies receptor-mediated inhibition of M currents. Neuron 2003;37:963–75.
[78] Zhao J, Pan HL, Li TT, Zhang YQ, Wei JY, Zhao ZQ. The sensitization of peripheral C-fibers to lysophosphatidic acid in bone cancer pain. Life Sci 2010;87:120–5.
[79] Zheng Q, Fang D, Cai J, Wan Y, Han JS, Xing GG. Enhanced excitability of small dorsal root ganglion neurons in rats with bone cancer pain. Mol Pain 2012;8:24–41.
[80] Zimmermann M. Ethical guidelines for investigations of experimental pain in conscious animals. PAIN® 1983;16:109–10.